Available online at www.sciencedirect.com
ScienceDirect
Trans. Nonferrous Met. Soc. China 24(2014) 2393−2400
Transactions of Nonferrous Metals Society of China
www.tnmsc.cn

Near net shape casting process for producing high strength 6xxx aluminum alloy automobile suspension parts

Shi-jie GUO, Yi XU, Yi Han, Jin-yan LIU, Guan-xia XUE, Hiromi NAGAUMI

Suzhou Research Institute for Nonferrous Metals, Suzhou 215026, China

Received 17 October 2013; accepted 5 May 2014

Abstract: The automobile suspension parts of a high strength 6xxx aluminum alloy were produced using a novel technique known as near net shape casting for forging stock preparation. Based on the outline dimension of the forging stock, the shape of the ingot was designed as the near net shape and its casting process was studied by the numerical simulation and experimental investigation. The results show that the shrinkage of the ingot was highly correlated to its shape parameters and could be successfully forecast by the stimulation model. The casting parameters of the near net shape ingot were optimized and the near net shape 6xxx aluminum alloy ingots free of defects were cast in the laboratory. In order to obtain high performance forged suspension parts, the hot compression tests of the ingot were carried out. The results show that the subgrain fraction of the forged ingot was strongly affected by Zener−Hollomon parameters (Z parameters). The intermediate Z parameters, 1.09×10^{16} s^{-1}, will contribute to the larger number fraction of subgrains inside the forged ingot, which contributes to the high performance of the forged products.
Key words: near-net shape; DC casting; Z parameter; subgrains; automobile suspension part; aluminum alloy

1 Introduction

In the automotive industry around the world, heavy cast iron and steel parts have been replaced with lightweight aluminum castings. Aluminum alloys with excellent characteristics related to lightness, high specific strength, and good corrosive resistance have been widely used for suspension parts connecting the front axle to the cross member [1−2].

In the traditional way to produce suspension parts, the aluminum alloys were firstly cast into billet and extruded to rods and bars. After four or five steps of ending and forging, the suspension parts of aluminum alloys were finally produced. In this way, the cost of the production process was high and the quality control of the products was difficult because of numerous processing steps. In order to reduce the mass of suspension parts and increase the quality of the product, an optimal process design from conception to manufacture was required [3]. Particularly, from a manufacturing point of view, for lighter and more advanced functional products, near net shape casting had substantial potential as an innovative manufacturing process to produce the forged products [4,5]. The concept of the near net shape casting was that the shape of the ingot was designed to be similar to the shape of the forged products and the ingot was produced by traditional DC (direct chill) casting. In this way, the forged billet could be produced directly by DC casting process without the extrusion and bending procedure. Compared with the traditional ways to produce suspension parts, the casting of the near net shape ingot provided a new way to produce the suspension parts of aluminum alloys.

In this work, the new method to produce the suspension parts was studied. The casting process of the near net shape ingot was investigated and the ingot was hot compressed at different Zener−Hollomon parameters. The properties of automobile suspension part produced by this new way were also measured and evaluated.

2 Experimental

The chemical composition for a newly developed 6xxx aluminum alloy used in this work was given in Table 1, which was protected by China patent [6]. Mg and Si elements were the main alloying elements in the 6xxx aluminum alloy, Mn and Cr elements were the microelements which suppress the recrystallization.

Corresponding author: Hiromi NAGAUMI; Tel: +86-512-88165012; E-mail: changhai_bw@sinr.cn
DOI: 10.1016/S1003-6326(14)63362-8

Table1 Chemical composition of 6xxx alloy (mass fraction, %)

Mg	Si	Cu	Mn	Cr	Fe	Ti	Al
0.8−1.4	0.8−1.6	0.2−0.8	0.6−1.0	0.1−0.3	≤0.25	≤0.1	Bal.

First of all, in order to design the outline dimension of the near-net shape ingot, the DC casting process of the ingot was calculated [7]. The hot top casting of the ingot was modeled and the shape of the ingot was designed by the simulation. Based on the simulated results, the casting parameters of near-net shape ingot were optimized and the ingots without defects were produced in our laboratory. Hot compression tests of the alloy were carried out on a Gleeble−3500 system at strain rates of 10^{-3} s^{-1}−1 s^{-1} and deformation temperatures of 350−550 °C. After obtaining the variation of subgrain fraction with different Zener−Hollomon parameters [8,9], the ingot was forged on the commercial forging machine and the properties of the suspension parts were investigated.

3 Results and discussion

3.1 Numerical procedures of modeling near-net shape ingot and casting results

The commercial software Procast was used to obtain the temperature field and the shrinkage of the ingot during the casting process. Figure 1 gives the designed shape of the forged ingot. Considering the solidification shrinkage and forging process, the mesh model of the near-net ingot was created, as shown in Fig. 2, which had the same geometry with the experimental equipments.

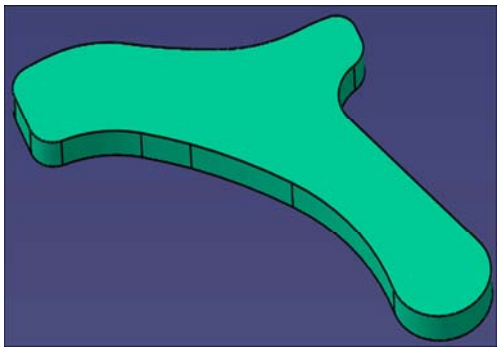

Fig. 1 External form of forging stock

According to the hydrodynamic law, the following conservation equations must be satisfied.

Conservation equation of mass:

$$\frac{\partial \rho}{\partial t}+\nabla\cdot(\rho U)=0 \tag{1}$$

Conservation equation of momentum:

$$\frac{\partial(\rho U)}{\partial t}+\nabla\cdot(\rho UU)=\nabla\cdot(\mu_{\text{eff}}\nabla U)-\nabla P+S_{\text{m}} \tag{2}$$

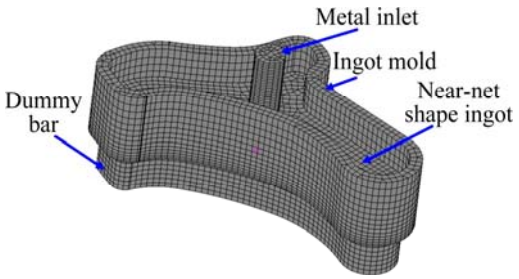

Fig. 2 Mesh model used in simulation

Conservation equation of energy:

$$\frac{\partial(\rho T)}{\partial t}+\nabla\cdot(\rho UT)=\nabla\cdot(\frac{k}{c_p}\nabla T)+S_{\text{th}} \tag{3}$$

where ρ is the density, μ_{eff} is the effective viscosity coefficient, k is the turbulence kinetic energy, c_p is the specific heat capacity, and S is the source item in Eqs. (2) and (3).

In this model, the standard k−ε model, which is a semi-empirical model, was used to model transport of turbulence kinetic energy (k) and its dissipation rate (ε). In the mushy region, the formation of dendrites will hinder the melt flow and the source item S is added to the momentum equation to consider this phenomenon.

The equation of source item S_{th} can be written as

$$S_{\text{th}}=[(1-\beta)^2/(\beta^3+\varepsilon)]A_{\text{mushy}}(v-v_{\text{p}}) \tag{4}$$

where A_{mushy} is a constant of mushy region, v_{p} is the casting speed and ε is the dissipation rate.

Moreover, the source item S_{m} is added to the momentum equation and can be written as

$$S_{\text{m}}=[(1-\beta)^2/(\beta^3+\varepsilon)]A_{\text{mushy}}\Phi \tag{5}$$

where Φ is the current kinetic trubulent energy.

3.2 Boundary conditions

When the flow field and thermal field are solved, the boundary conditions are described as follows: inlet boundary Γ_1, free surface boundary Γ_2, hot top boundary Γ_3, primary cooling boundary Γ_4, secondary cooling boundary Γ_5, and outlet boundary Γ_6. The boundary conditions are shown in Fig. 3.

Inlet boundary Γ_1: The inlet velocity is related to the casting speed, which satisfies the law of mass conservation. The turbulence kinetic energy k and its dissipation rate ε can be described as

$$k=0.01\times u_{\text{inlet}}^2 \tag{6}$$

$$\varepsilon=k^{1.5}/R_{\text{inlet}} \tag{7}$$

where u_{inlet} is the inlet velocity and R_{inlet} is the hydraulic radius of the inlet.

Free surface boundary Γ_2 and hot top boundary Γ_3:

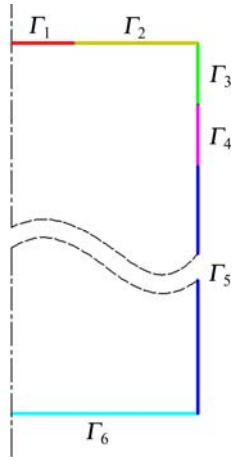

Fig. 3 Boundary conditions used in this model

In this boundary the heat loss by emission is quite small which can be neglected. The free surface is treated as the adiabatic wall.

Primary cooling boundary Γ_4: The velocity and turbulence boundary conditions are set to the static wall and the thermal boundary condition is treated as Cauchy type boundary condition, which can be formulated as follows:

$$-\lambda\left(\frac{\partial T}{\partial n}\right)_{\mathrm{w}} = h(T_{\mathrm{w}} - T_{\mathrm{en}}) \tag{8}$$

where λ is the heat conductivity of the material, h is the coefficient of heat transfer, T_{w} is the temperature of the static wall and T_{en} is the ambient temperature.

In the primary cooling boundary, the heat coefficient between the mold and the melt is assumed to be varied with the solid fraction and is written as follows:

$$h = h_{\mathrm{contact}} \times (1 - f_{\mathrm{s}}) + h_{\mathrm{gap}} \times f_{\mathrm{s}} \tag{9}$$

where h_{contact} is given as 2500 W/(m^2·K) to reflect good thermal contact between the mold and the ingot and h_{gap} is equal to 50 W/(m^2·K) to reflect poor thermal contact associated with the air gap formed when the melt is solidified. The solid fraction f_{s} is formulated as follows:

$$f_{\mathrm{s}} = \begin{cases} 0, & T \geq T_{\mathrm{liquid}} \\ \dfrac{1}{1-k_{\mathrm{p}}} \times \dfrac{T_{\mathrm{liquid}} - T}{T_{\mathrm{f}} - T}, & T_{\mathrm{liquid}} \geq T \geq T_{\mathrm{solid}} \\ 1, & T \leq T_{\mathrm{solid}} \end{cases} \tag{10}$$

where T_{f} is the fusion temperature of the pure base metal and k_{p} is the solute partition coefficient. The heat transfer coefficients of primary cooling boundary can be defined by using Procast User Functions.

Secondary cooling boundary Γ_5: The boundary is divided into two zones where are the impingement zone and the streaming zone. They are also Cauchy type boundary conditions and the heat coefficient in the impingement zone is much larger than that of the streaming zone. Moreover, the temperature of the cooling water is the function of position of the ingot, which is shown in Fig. 4. In the impingement zone, the temperature of cooling water remains constant. However, in the streaming zone, the temperature of cooling water exhibits a linear increase at first and then reaches a constant value. The heat transfer coefficient of secondary cooling boundary can also be defined by using Procast User Functions.

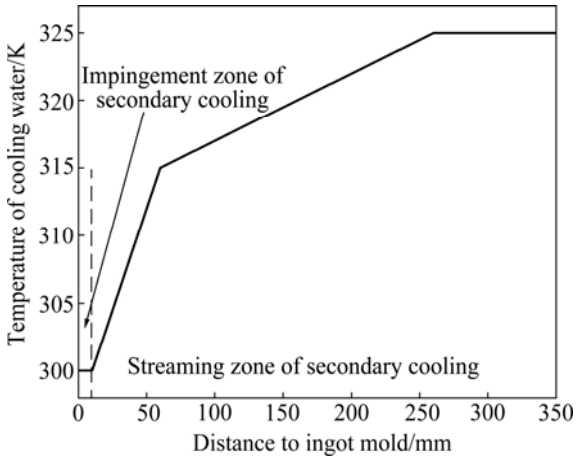

Fig. 4 Temperature of cooling water in secondary cooling zone

Outlet boundary Γ_6: The outlet velocity is equal to the casting speed and the thermal boundary is treated as the Dirichlet type boundary in which the temperature is constant value.

3.3 Material parameters

The liquidus and solidus temperatures of the newly developed 6xxx alloy used in this work are 654 °C and 547 °C, respectively. The thermal mechanical properties of the 6xxx alloy used in the model are given in Figs. 5−10. The thermal conductivity and enthalpy of the

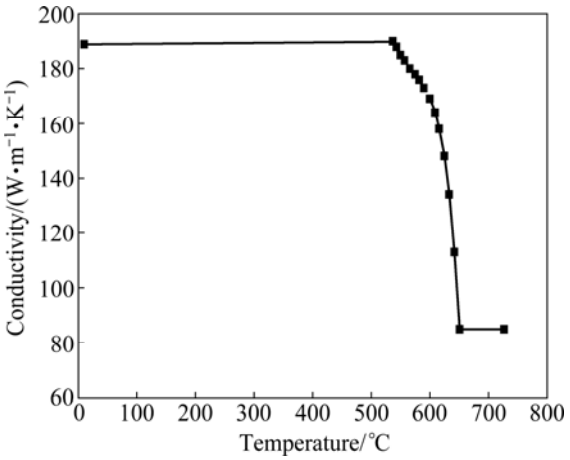

Fig. 5 Thermal conductivity of 6xxx alloy

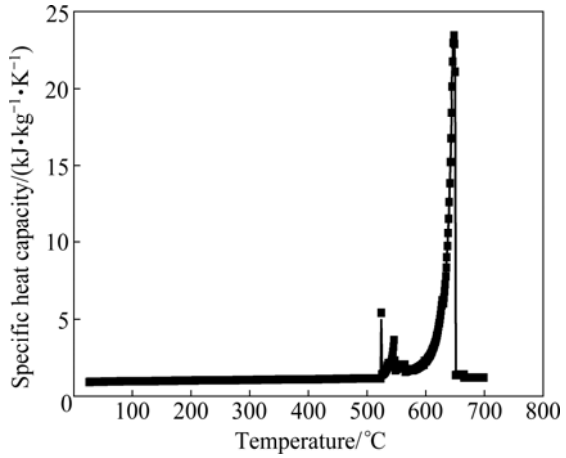

Fig. 6 Specific heat capacity of 6xxx alloy

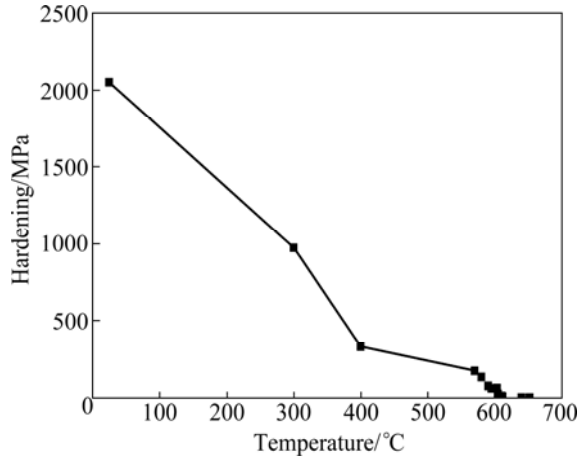

Fig. 7 Hardening curve of 6xxx alloy

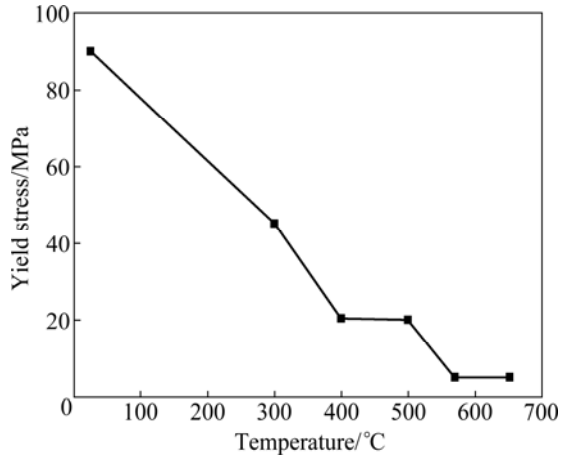

Fig. 8 Yield stress of 6xxx alloy

the alloy during the solidification are based on the Scheil model [10]. The equivalent specific heat capacity method was applied to analyzing the solidification latent heat during the casting.

In order to test the simulated results, the temperature measurement was implemented by implanting thermocouples into the withdrawing billet during the casting process. Two thermocouples at point *A* and point *B*, shown in Fig. 11, were embedded into the ingot and solidified during the casting. Figure 12 gives the comparisons of the temperature histories between the calculated results and the measurements. It shows that there is a good agreement between the calculated results and the measured results. These results indicate that the mathematical model, material parameters and boundary conditions used in the simulation are accurate and the model can be applied to simulating the casting process of the ingot.

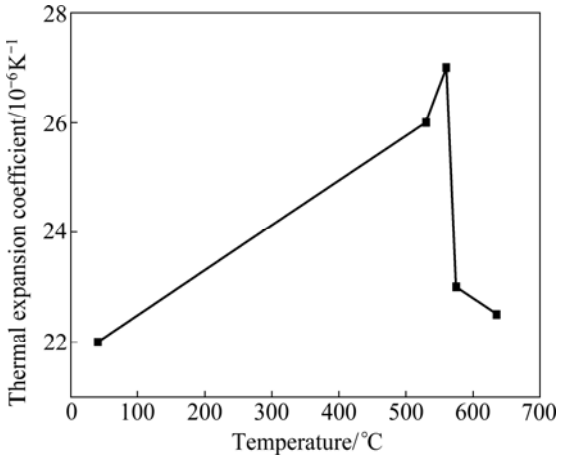

Fig. 9 Thermal expansion coefficient of 6xxx alloy

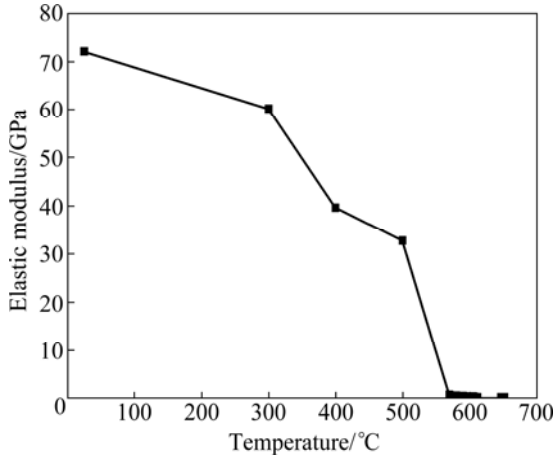

Fig. 10 Elastic modulus of 6xxx alloy

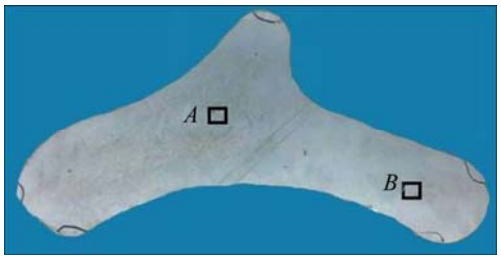

Fig. 11 Embedded points of thermocouples inside ingot

Figure 13 shows the calculated temperature field of the near-net shape ingot during the casting process. Because of the heat transfer between the cooling water and liquid metal, the molten aluminum solidifies and

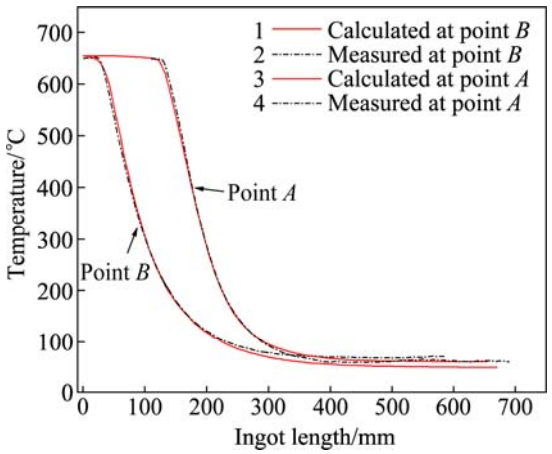

Fig. 12 Comparison of temperature histories between calculated and measured results

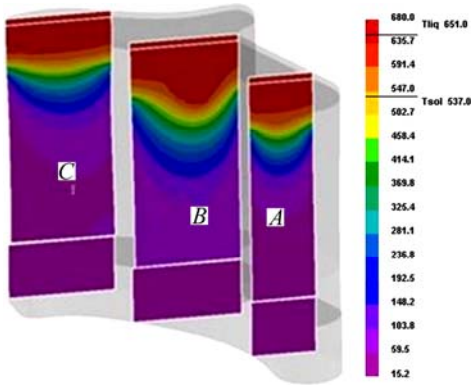

Fig. 13 Temperature distribution inside near-net shape ingot

forms a solid layer attached to the mold. The temperature of melt inside the hot top changes from 680 °C to 700 °C due to the heat insulation material. Because of the ingot shape difference, the temperature distribution at different positions of the ingot changes significantly under the external cooling conditions. At the positions of section *A* and section *C*, which are close to the ingot edge, there is a small difference between the edge and the center and the depth of the sump is 2.5 mm. However, at the position of section *B*, which is closer to the ingot center, there is a big difference between the edge and the center and the sump depth changes to 6.4 mm. That is to say, the melt at the section *A* and section *C* solidifies much quicker than that at section *B*. The difference on the solidification rate inside the ingot may affect the shrinkage direction.

Figure 14 shows the ingot shrinkage indication after the casting. Obviously, the shrinkage direction is closely associated with the ingot shape. The authors consider that the shrinkage is correlated with the cooling conditions of the ingot [7]. In the current cooling conditions excessive solidification shrinkage happens at the regions of the ingot marked *A*, *B* and *C*, shown in Fig. 14. The outline of the solidified ingot is over the mold boundary, which will increase the friction force between the ingot and the mold wall significantly. The increased friction force will result in a reaction force to the ingot. Cracks will occur if the reaction force is larger than the material strength. Figure 15 shows the cast ingot where the solidification conditions are the same as that used in the simulation. Cracks defects are observed on the ingot. Therefore, cooling conditions of the ingot must be changed to suppress the defects. The cooling conditions of the ingot were changed by changing the casting parameters and modifying the cooling water distribution. The near-net shape ingot without the defects was successfully cast in our laboratory, as shown in Fig. 16. The ingot is 2.2 m in length and the quality is good for forge work.

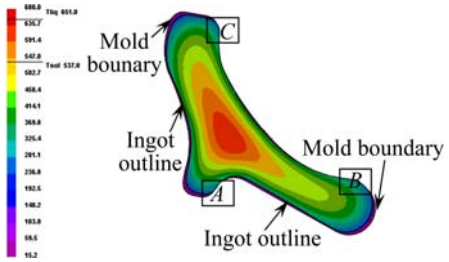

Fig. 14 Ingot shrinkage during casting

Fig. 15 Casting defects inside ingot

Fig. 16 Near-net shape ingot cast in our laboratory

3.4 Microstructure evolution after hot compression

Microstructural evolution of several series aluminum alloys during hot deformation has been investigated by some researchers [11−13]. The 6xxx alloy is a Al−Mg−Si−Cu alloy newly developed by our group and the microstructure evolution after hot compression was investigated in this section.

In order to improve the performance of aluminum structural material, abnormal grain growth (AGG) during thermo-mechanical processing should be avoided. The grain coarsening is more critical with the increase of the Z parameter, which results from the occurring of AGG. It is generally accepted that the deformed microstructure which consists of subgrains has higher strength [14−17]. Therefore, the changes of subgrains during the hot deformation and treatment were investigated.

Figure 17 shows the OIM pictures of deformed microstructure. The values of Z parameter which is used to characterize the combined effects of strain rate and deformation temperature are from 7.01×10^{12} s^{-1} to 8.57×10^{20} s^{-1} in this study. Under large Z parameters of 8.57×10^{20} s^{-1}, a large number of subgrains are observed in elongated grains and the percentage of subgrains is 64.30%. With Z parameter value decreasing from 1.09×10^{16} s^{-1} to 7.01×10^{12} s^{-1}, proceeding of dynamic recrystallization (DRX) is more adequate. It can be seen that subgrains and recrystallized grains coexist. The percentages of subgrains are 54.98% and 25.12%, respectively.

Figure 18 shows the OIM pictures after (560 °C, 1 h) solution heat treatment (SHT). The grains become coarse seriously because of abnormal grain growth and there are some island grains in the abnormally large grains after SHT with large Z parameter of 8.57×10^{20} s^{-1}. After the heat treatment, the percentage of subgrains is decreased to 18.95%. Under the intermediate and small Z parameters

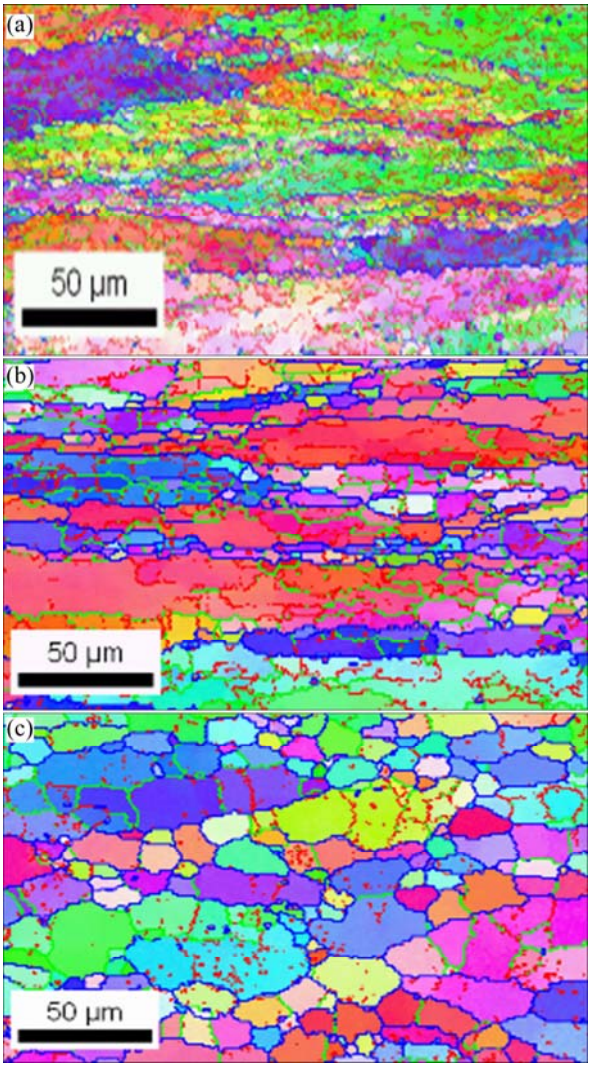

Fig. 17 OIM micrographs of alloy compressed under different Z parameters: (a) 8.57×10^{20} s^{-1} (350 °C, $\dot{\varepsilon}=1$ s^{-1}); (b) 1.09×10^{16} s^{-1} (450 °C, $\dot{\varepsilon}=10^{-2}$ s^{-1}); (c) 7.01×10^{12} s^{-1} (550 °C, $\dot{\varepsilon}=10^{-3}$ s^{-1})

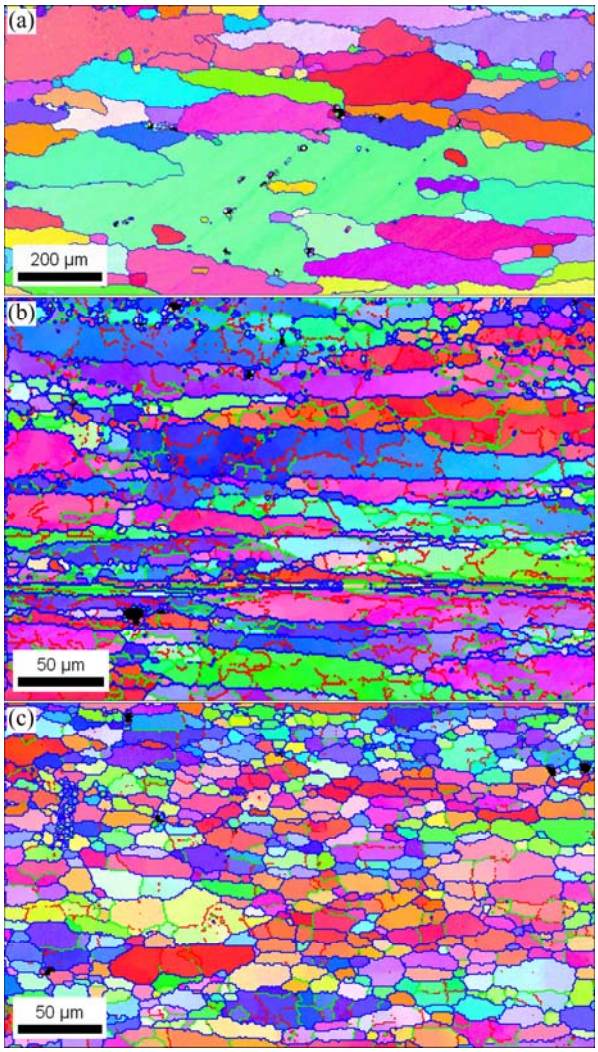

Fig. 18 OIM micrographs of alloy after (560 °C, 1 h) SHT with different Z parameter: (a) 8.57×10^{20} s^{-1} (350 °C, $\dot{\varepsilon}=1$ s^{-1}); (b) 1.09×10^{16} s^{-1} (450 °C, $\dot{\varepsilon}=10^{-2}$ s^{-1}); (c) 7.01×10^{12} s^{-1} (550 °C, $\dot{\varepsilon}=10^{-3}$ s^{-1})

of 1.09×10^{16} s^{-1} and 7.01×10^{12} s^{-1}, the microstructures are stable apparently because the stored energy is not high enough to cause recrystallization, and the percentages of subgrains are changed to 69.9% and 29.6% at the current treatment conditions, respectively. Obviously, the material exhibits large percentage of subgrains at the intermediate Z parameter of 1.09×10^{16} s^{-1}. Therefore, in the following forge work, we controlled the Z parameter changing around 1.09×10^{16} s^{-1} to obtain the forged product with higher subgrains percentage.

The slice of the near-net shape ingot was forged at the Z parameter around 1.09×10^{16} s^{-1} and the product of automobile suspension part is given in Fig. 19. No abnormal grain growth was observed in the product. The properties of the product at the regions of strengthening rib and web plate are given in Table 2. Good performance was obtained in our product of automobile suspension part.

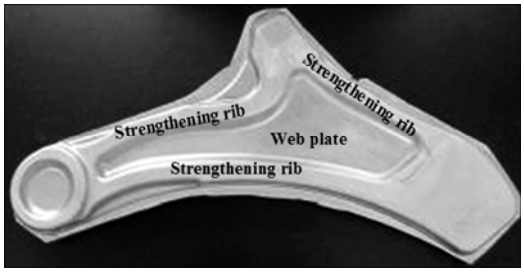

Fig. 19 Product of automobile suspension part

Table 2 Mechanical properties of automobile suspension part

Position	Yield strength/MPa	Tensile strength/MPa	Elongation/%
Strengthening rib	386.5	413.0	11.8
Web plate	386.0	410.5	12.5

4 Conclusions

1) The casting process of the near-net shape ingot was studied by the numerical simulation and experimental investigation. The ingot shrinkage was closely associated with its shape and cooling conditions.

2) Based on the stimulation model, the temperature field and shrinkage of the near-net shape ingot were calculated and the ingot free of defects was cast. Hot compression tests of 6xxx aluminum alloy were carried out and the results showed that the subgrain fraction of the forged ingot was affected by Zener−Hollomon parameters.

3) The material exhibited large subgrains percentage at the intermediate Z parameter, 1.09×10^{16} s^{-1}, before and after solution heat treatment. The forged automobile suspension part with high mechanical properties was produced by near-net shape ingot successfully.

References

[1] THAM L M, GUPTA M, CHENG L. Influence of processing parameters on the near-net shape synthesis of aluminium-based metal matrix composites [J]. Journal of Materials Processing Technology, 1999, 89: 128−134.

[2] GUPTA M, LING S. Microstructure and mechanical properties of hypo/hyper-eutectic Al−Si [J]. J Alloys Compd, 1999, 287: 284−294.

[3] MILLER W S, ZHUANG L, BOTTEMA J, WITTEBROOD A J, SMET P, HASZLER A, VIEREGGE A. Recent development in aluminium alloys for the automotive industry [J]. Mater Sci Eng A, 2000, 280: 37−49.

[4] ZHANG Xing-zhong. Development of near-net-shape continuous casting for beam blank [J]. Iron and Steel, 1996, 31(12): 72−75.

[5] FENG Qi. The Development of near-net-shape CC and new ironmaking technology [J]. Anhui Metallurgy, 2008(3): 21−23. (in Chinese)

[6] HAN Yi, MA Ke, WANG Chu-yan. A high strength Al−Mg−Si−Cu alloy and preparation method: China, 201210240858.6 [P]. 2012−10. (in Chinese)

[7] NAGAUMI H, TAKEDA Y, UMEDA T. FEM simulation in the casting process of neat net shape DC billet [J]. Journal of Japan Institute of Light Metals, 2005, 55(10): 463−467.

[8] SHEPPARD T. Prediction of structure during shaped extrusion and subsequent static recrystallization during the solution soaking operation [J]. Journal of Material Processing Technology, 2006, 177: 26−35.

[9] ZHANG Hui, LI Luo-xing, YUAN Deng, PENG Da-shu. Hot deformation behavior of the new Al−Mg−Si−Cu aluminum alloy during compression at elevated temperatures [J]. Material Characterization, 2007, 58: 168−173.

[10] ZHANG Hai-tao. Macrophysical fields in low frequency electro-magnetic casting of aluminum alloys [D]. Shenyang: Northeastern University, 2007. (in Chinese)

[11] HUANG Chang-qing, DIAO Jin-peng, DENG Hua, LI Bing-ji, HU Xing-hua. Microstructure evolution of 6016 aluminum alloy during compression at elevated temperatures by hot rolling emulation [J]. Transactions of Nonferrous Metals Society of China, 2013, 23: 1576−1582.

[12] HUANG Xu-dong, ZHANG Hui, HAN Yi, WU Wen-xiang, CHEN Jiang-hua. Hot deformation behavior of 2026 aluminum alloy during compression at elevated temperature [J]. Mater Sci Eng A, 2010, 527: 485−490.

[13] ZHANG Hui, LI Luo-xing, YUAN Deng, PENG Da-shu. Hot deformation behavior of the new Al–Mg–Si–Cu aluminum alloy during compression at elevated temperatures [J]. Materials Characterization, 2007, 58: 168−173.

[14] INAGAKI Y, FUKUDA A. Weight reduction of forged-aluminum automotive suspension [J]. Kobe Steel Engineering Reports, 2009, 59(2): 22−26.

[15] PANIGRAHI S K, JAYAGANTHAN R. Development of ultrafine grained Al–Mg–Si alloy with enhanced strength and ductility [J]. J

Alloys Compd, 2009, 470: 285−288.

[16] van GEERTRUYDEN W H, MISIOLEK W Z, WANG P T. Grain structure evolution in a 6061 aluminum alloy during hot torsion [J]. Mater Sci Eng A, 2006, 419: 105−114.

[17] HAN Yi, MA Ke, LI Lian, CHEN Wei, NAGAUMI Hiromi. Study on microstructure and mechanical properties of Al−Mg−Si−Cu alloy with high manganese content [J]. Materials and Design, 2012, 39: 418−424.

采用近终形铸造制备高强 6xxx 铝合金控制臂

郭世杰，徐 义，韩 逸，刘金炎，薛冠霞，长海博文

苏州有色金属研究院有限公司，苏州 215026

摘 要：采用近终形铸锭配合热锻工艺制备高强 6xxx 铝合金控制臂。首先设计近终形铝合金锭坯的形状，采用 Procast 商业软件模拟研究近终形铝合金铸锭的铸造过程。结果表明，近终形铝合金铸锭的收缩行为与铸锭形状相关，经模拟计算优化后，铸造出无缺陷的近终形 6xxx 铝合金铸锭。为了获得优异的锻件性能，研究了 6xxx 铝合金的热压缩行为。结果表明，锻件组织中的亚晶百分数与 Z 参数值相关；中等 Z 参数(1.09×10^{16} s^{-1})有利于获得较高的亚晶百分数，从而保证锻件产品具有更优的性能。

关键词：近终形；DC 铸造；Z 参数；亚晶；汽车控制臂；铝合金

(Edited by Sai-qian YUAN)